Supplementary Material

Ru@Ni_3S_2 Nanorod Arrays as Highly Efficient Electrocatalysts for Alkaline Hydrogen Evolution Reaction

Kefeng Wang,[a*] Bin Li,[a, b] Jingxiao Ren,[a] Wenxia Chen,[a] Jinhai Cui,[a] Wei Wei,[a] Peng Qu[a, b*]

[a] *Henan Engineering Center of New Energy Battery Materials, College of Chemistry and Chemical Engineering, Shangqiu Normal University, Shangqiu 476000, Henan, China*

[b] *College of Chemistry, Zhengzhou University, Zhengzhou 450002, China*

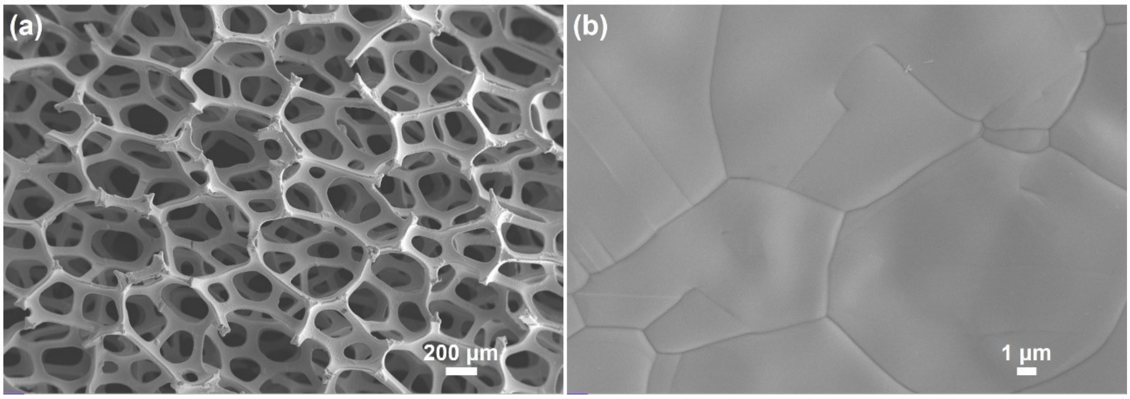

Figure S1 SEM images of blank nickel foam

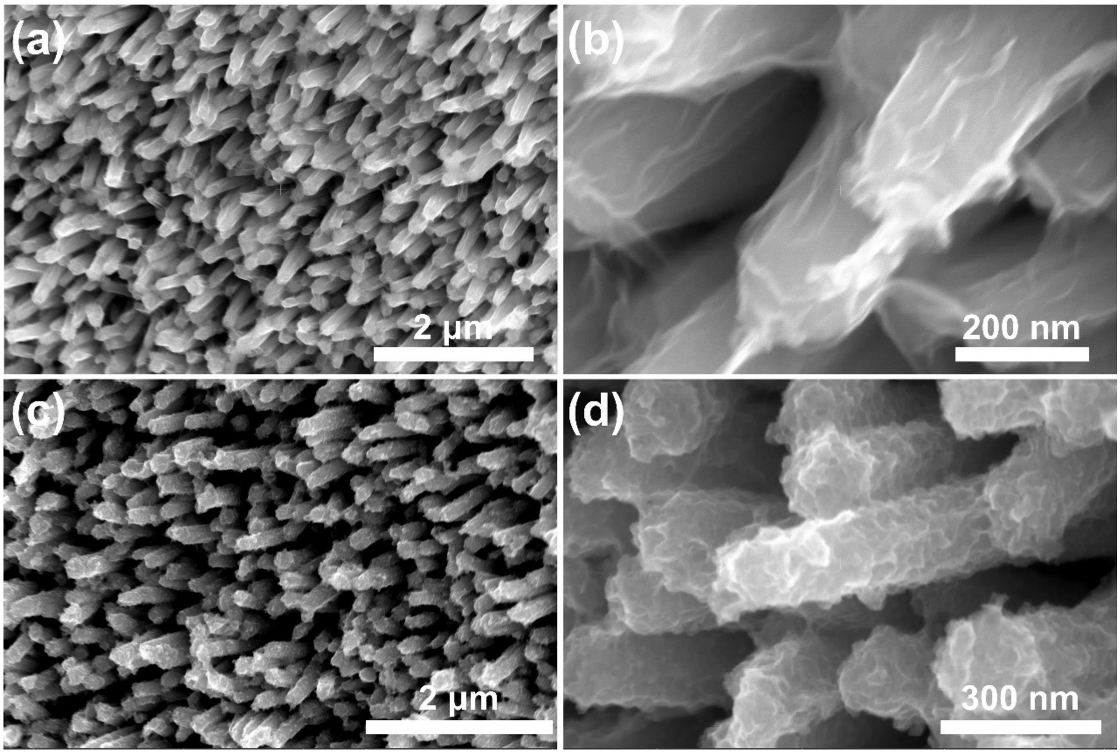

Figure S2 SEM images of Ni_3S_2/NF (a, b) and Ru@Ni_3S_2 (c, d) with different magnifications

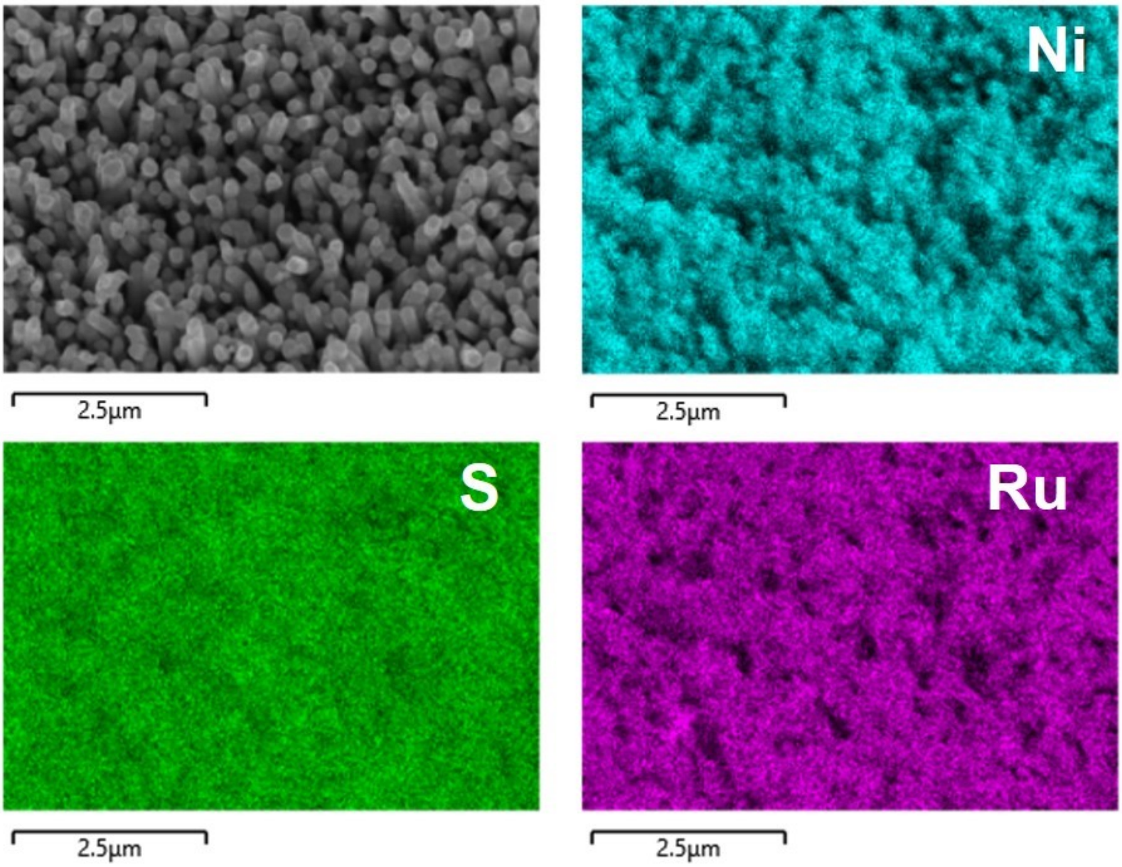

Figure S3 SEM image and corresponding EDS mapping images of Ru@Ni_3S_2

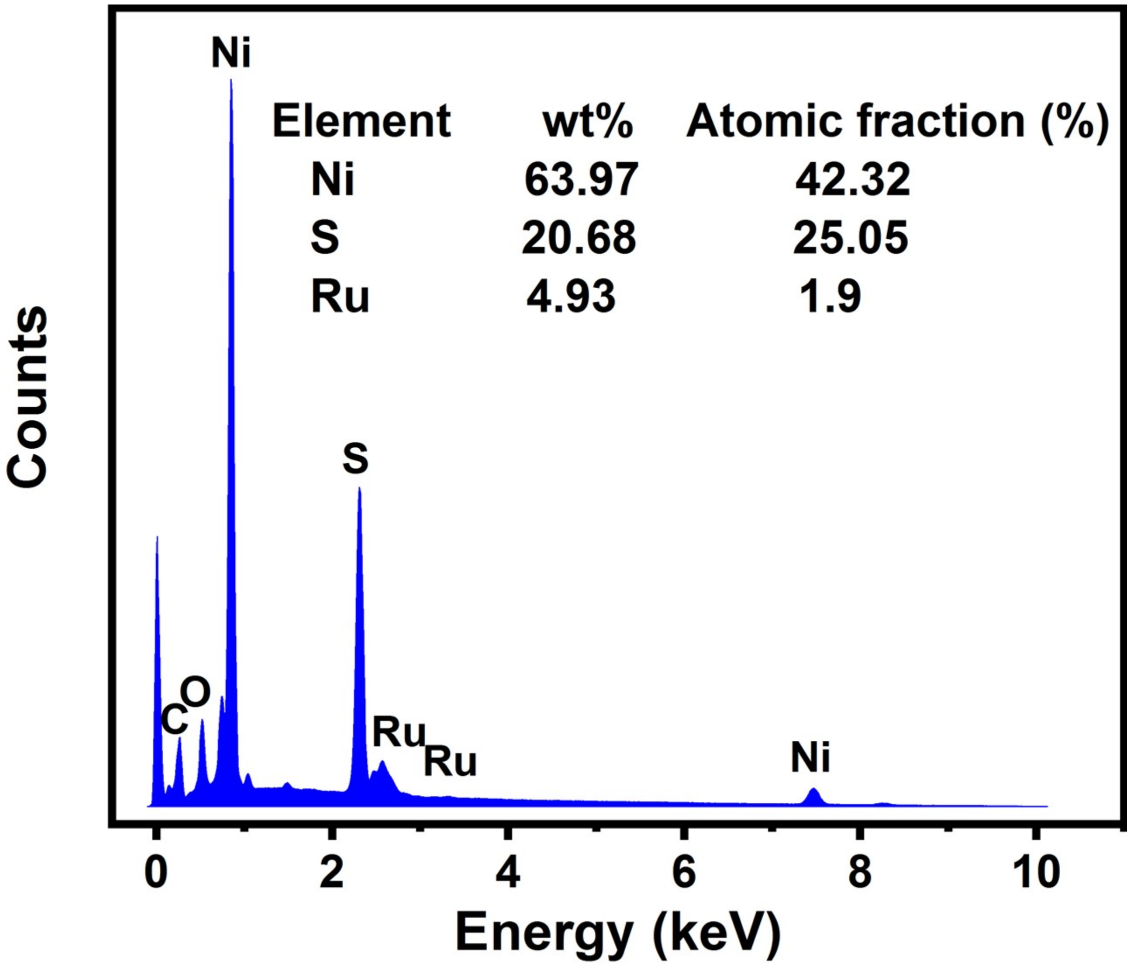

Figure S4 EDS spectrum of Ru@Ni_3S_2 and the corresponding elemental contents.

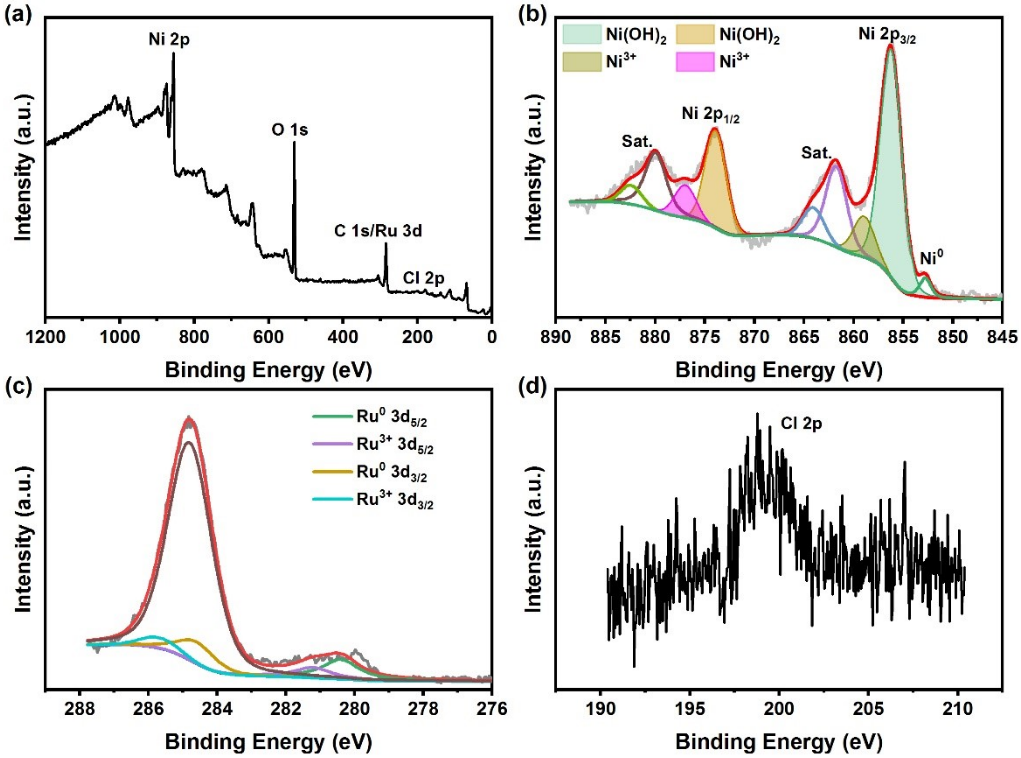

Figrue S5 XPS spectra of Ru/NF, (a) survey spectrum, (b, c, d) high-resolution Ni 2p, Ru 3d and Cl 2p spectra.

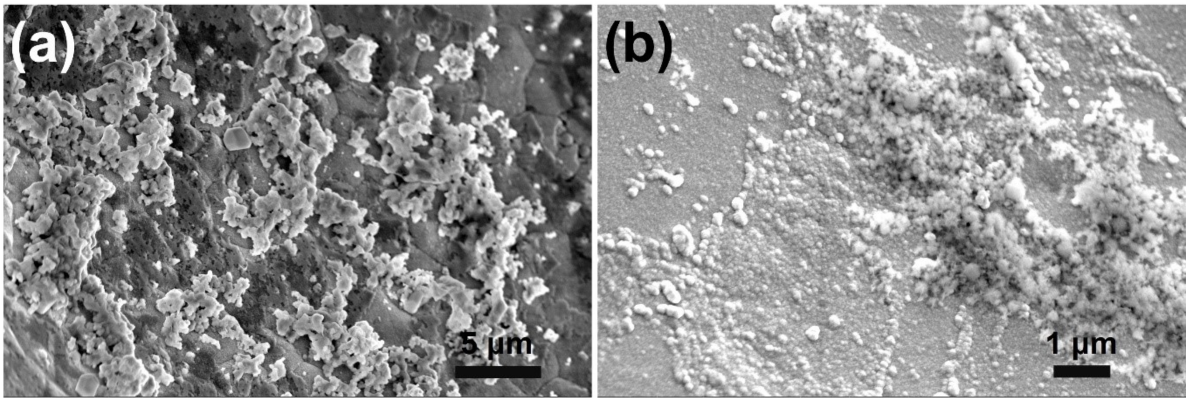

Figure S6 SEM images of Ru nanoparticles directly deposited on nickel foam (Ru/NF).

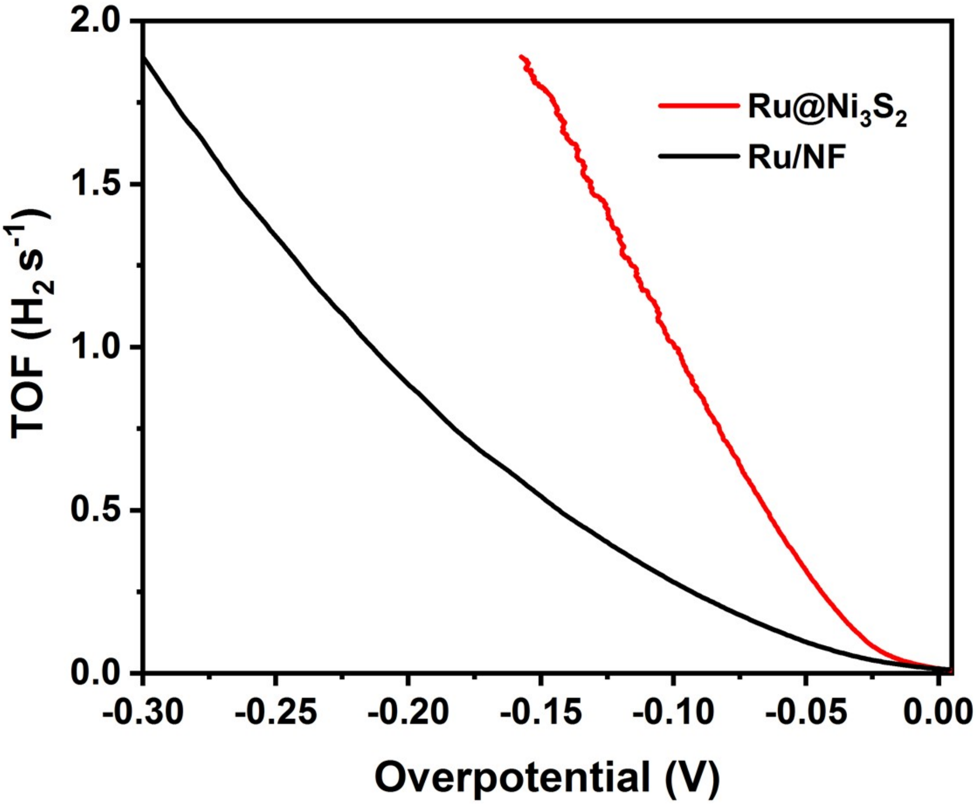

Figure S7 Comparison of TOF values at different overpotentials of $Ru@Ni_3S_2$ and Ru/NF

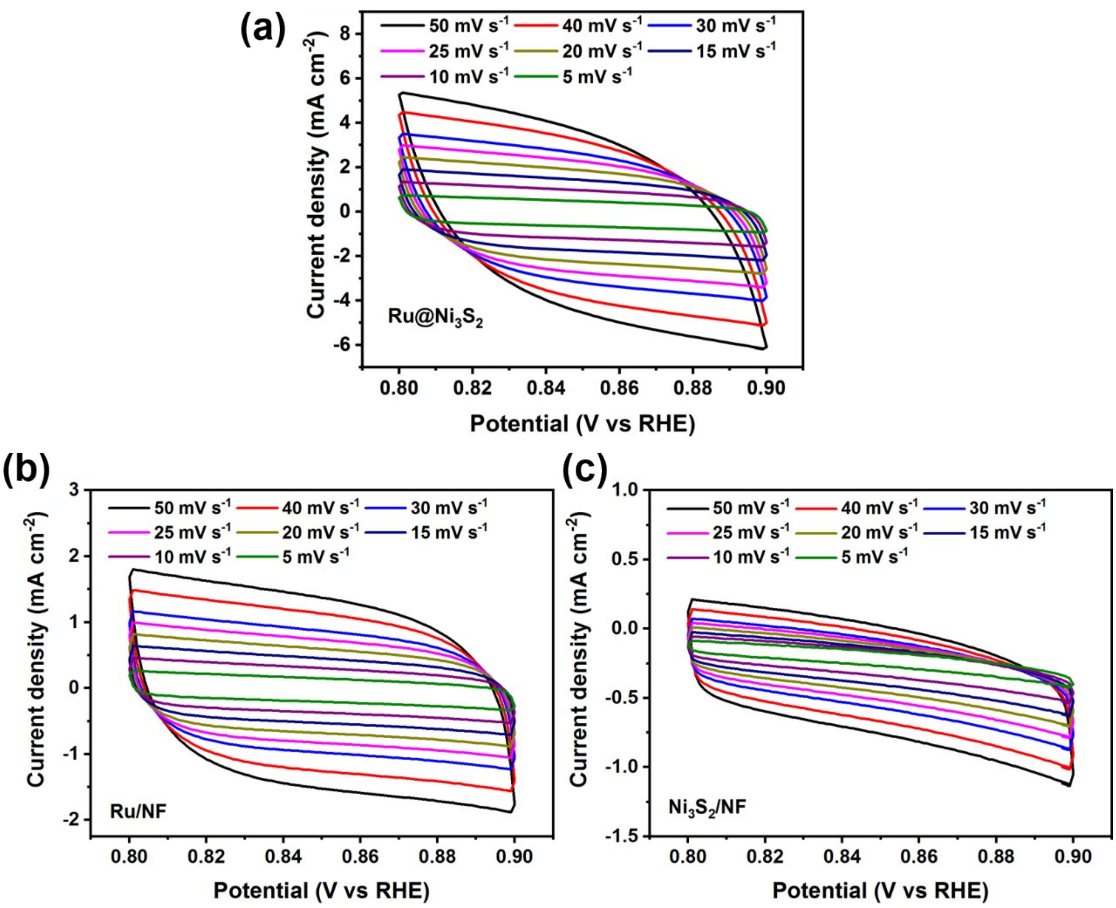

Figure S8 Cyclic voltammetry curves of Ru@Ni_3S_2, Ru/NF and Ni_3S_2/NF at different scan rates ranging from 5 mV s^{-1} to 50 mV s^{-1}.

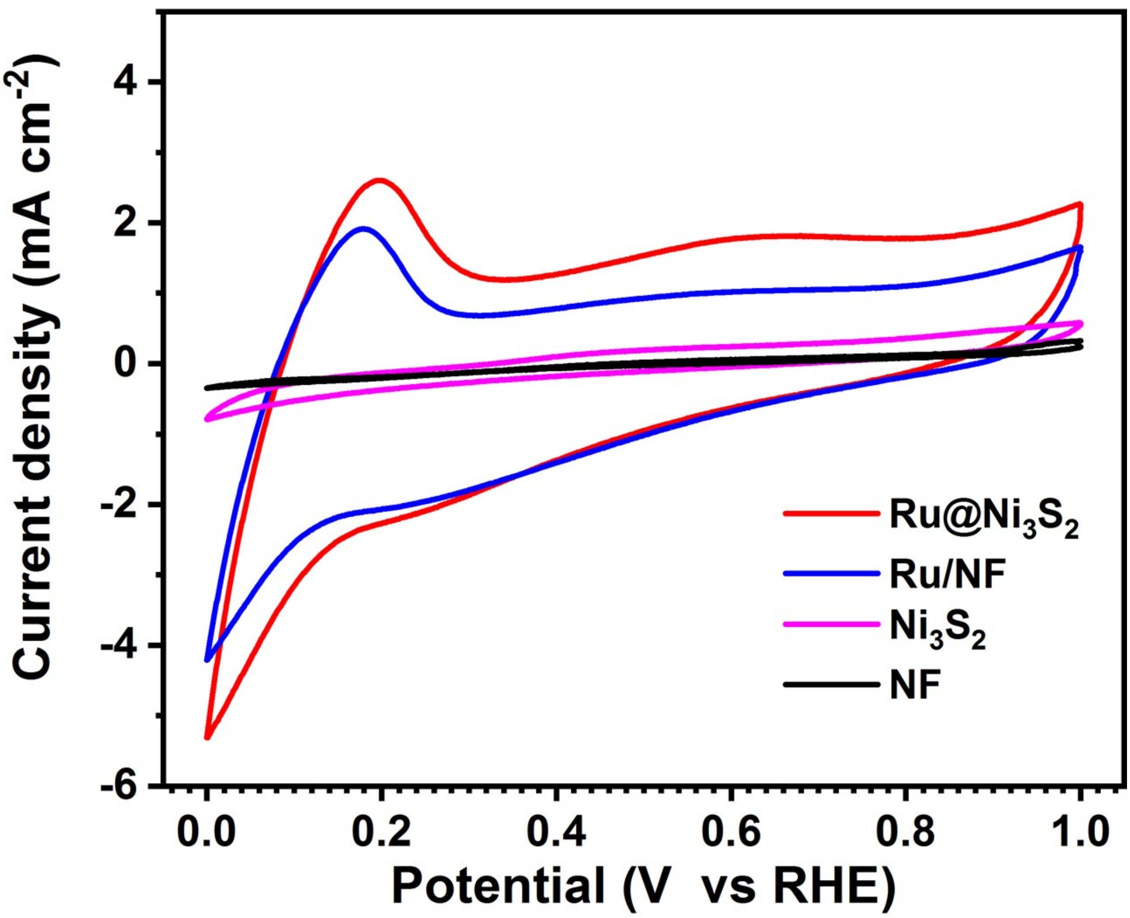

Figure S9 Cyclic voltammetry (CV) curves of different catalysts recorded in 0.1 M KOH electrolyte at a scan rate of 5 mV s^{-1}.

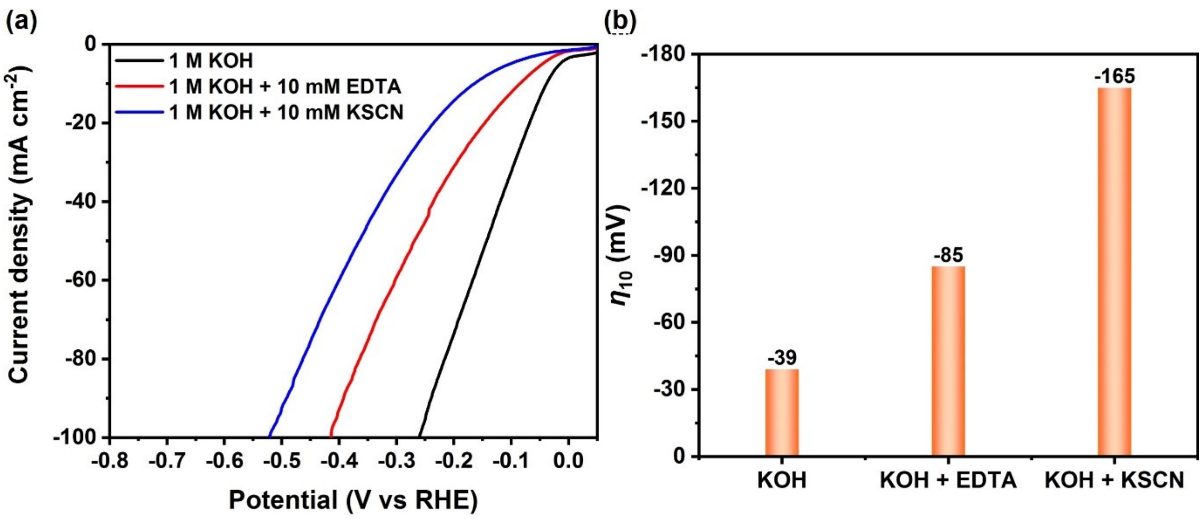

Figure S10 (a) LSV curves (without IR-compensation) for Ru@Ni_3S_2 in 1 mol/L KOH with the addition of 10 mmol/L EDTA or 10 mmol/L KSCN. (b) The corresponding overpotentials to deliver a current density of 10 mA cm^{-2}.

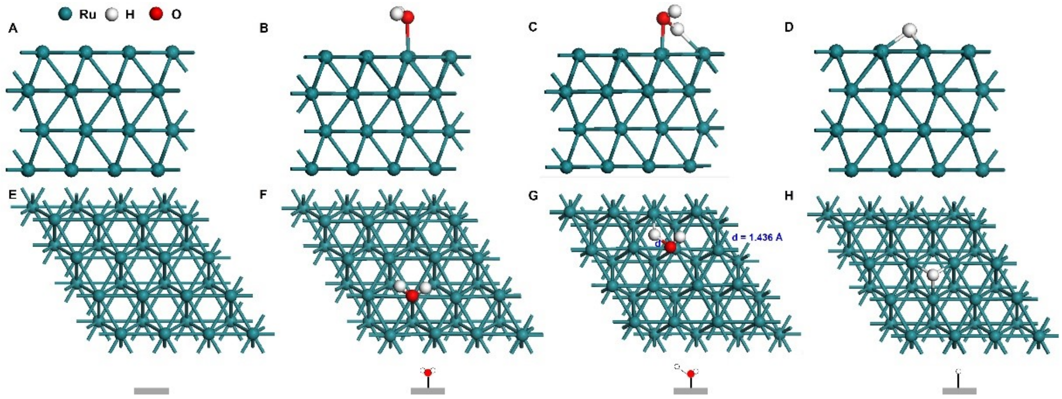

Figure S11 Optimized structure models of Ru(001) at different stages during the HER process.

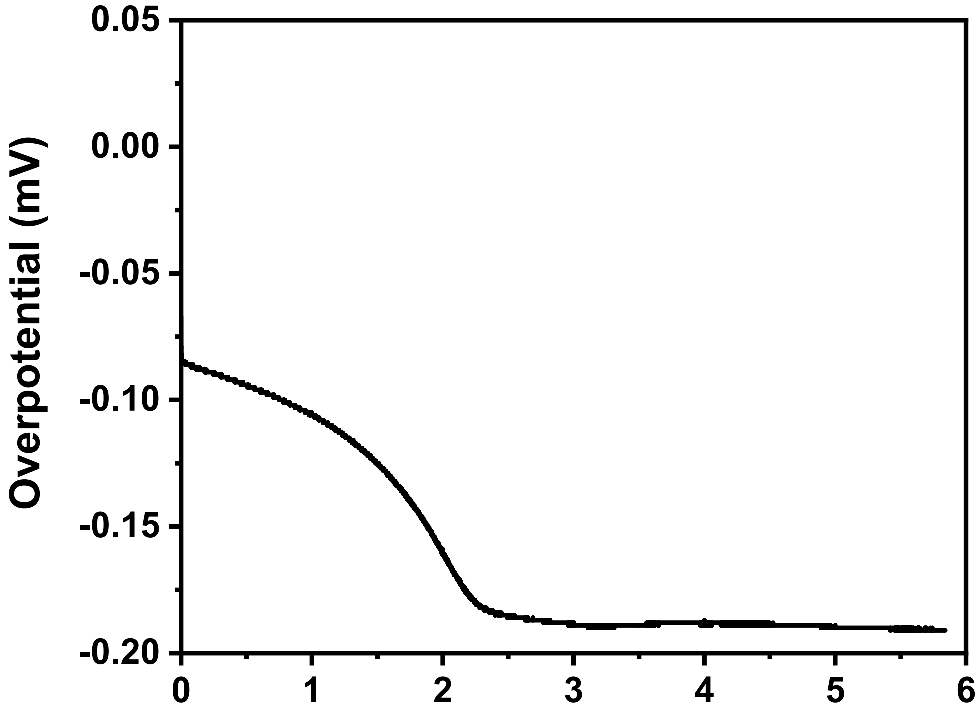

Figure S12 Long-term stability of Ru@Ni_3S_2 by recording the overpotential variation at a constant current density of 20 mA cm^{-2}.

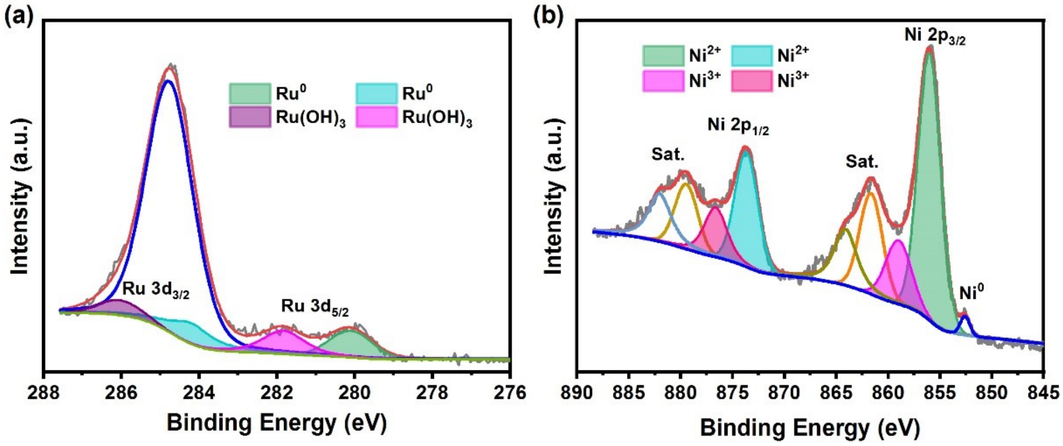

Figure S13 High-resolution XPS spectra of Ru 3d and Ni 2p for Ru@Ni_3S_2 after stability test.

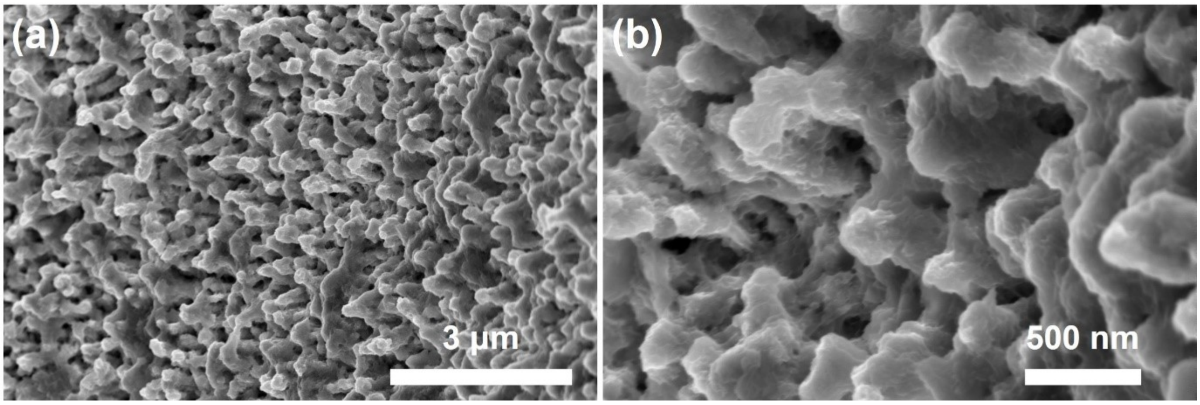

Figure S14 SEM images of Ru@Ni_3S_2 after long-term durability test.

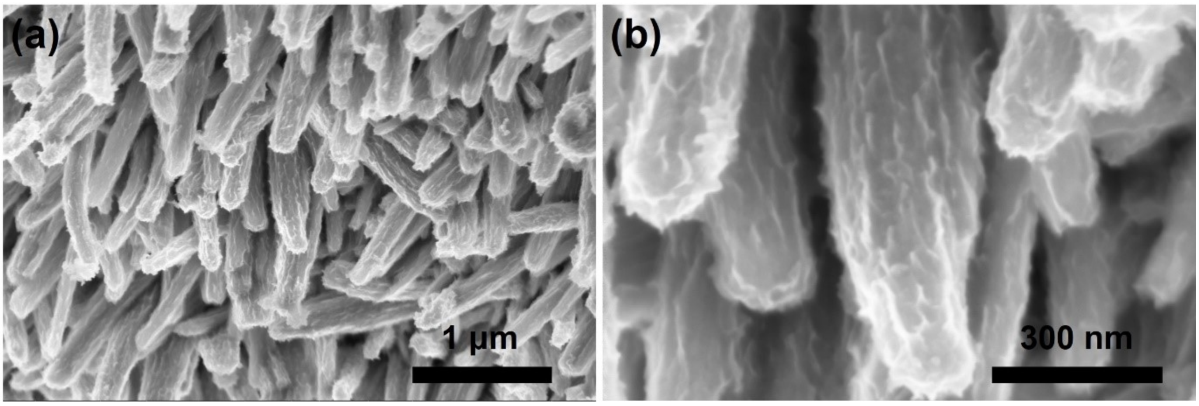

Figure S15 SEM images of Ni_3S_2/NF after long-term durability test.

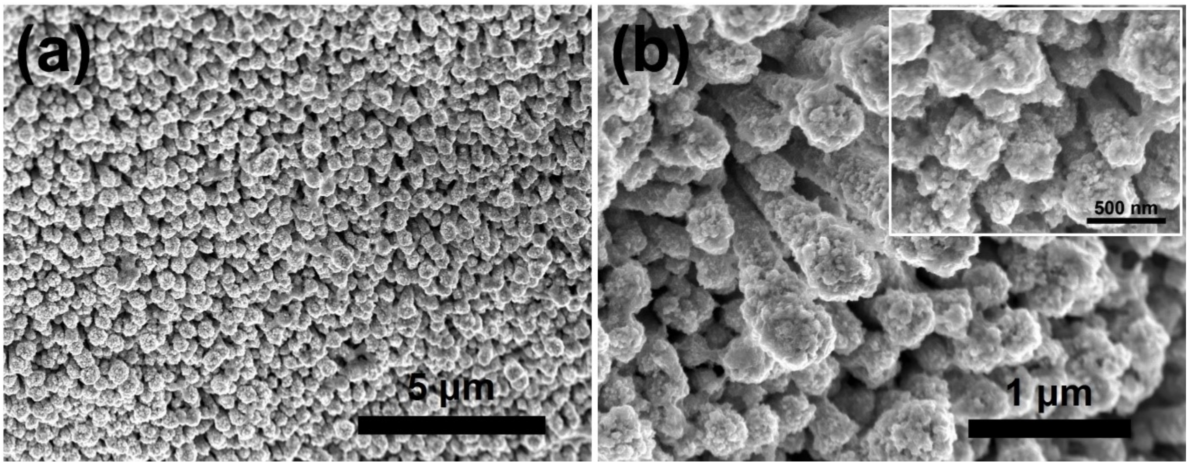

Figure S16 SEM images of PANI-Ru@Ni_3S_2

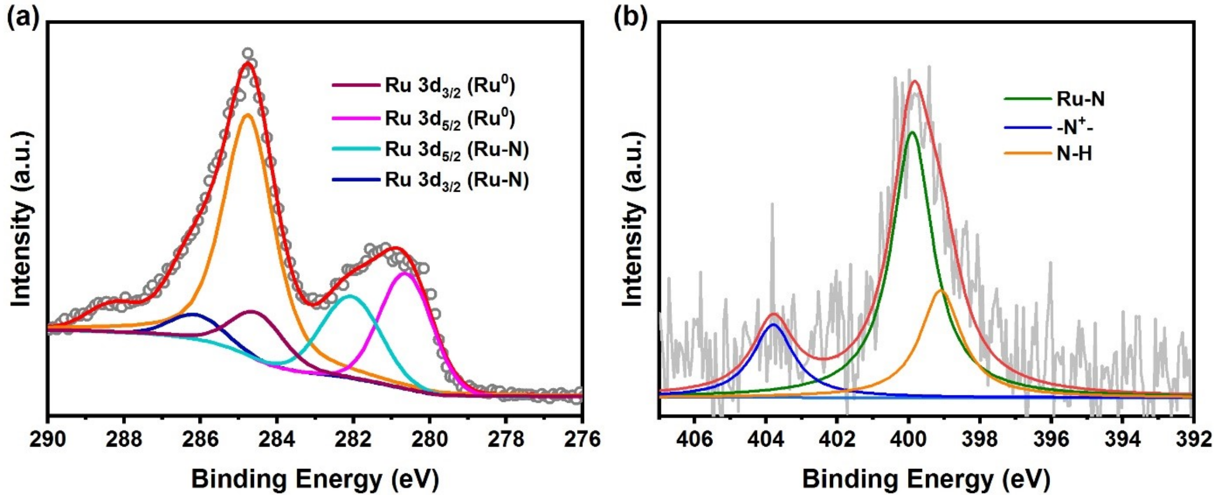

Figure S17 High-resolution Ru 3d and N 1s spectra of PANI-Ru@Ni_3S_2

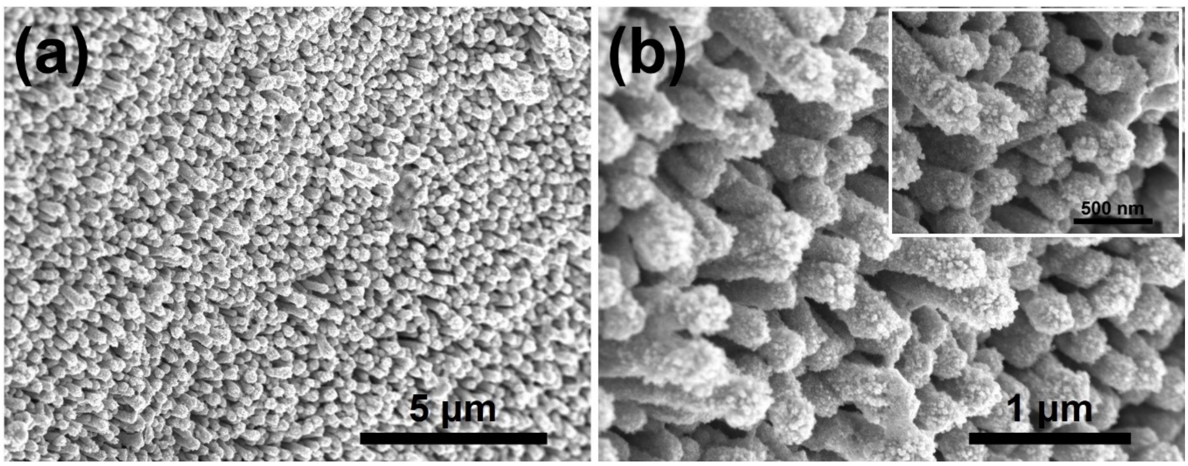

Figure S18 SEM images of PANI-Ru@Ni_3S_2 after long-term stability test.

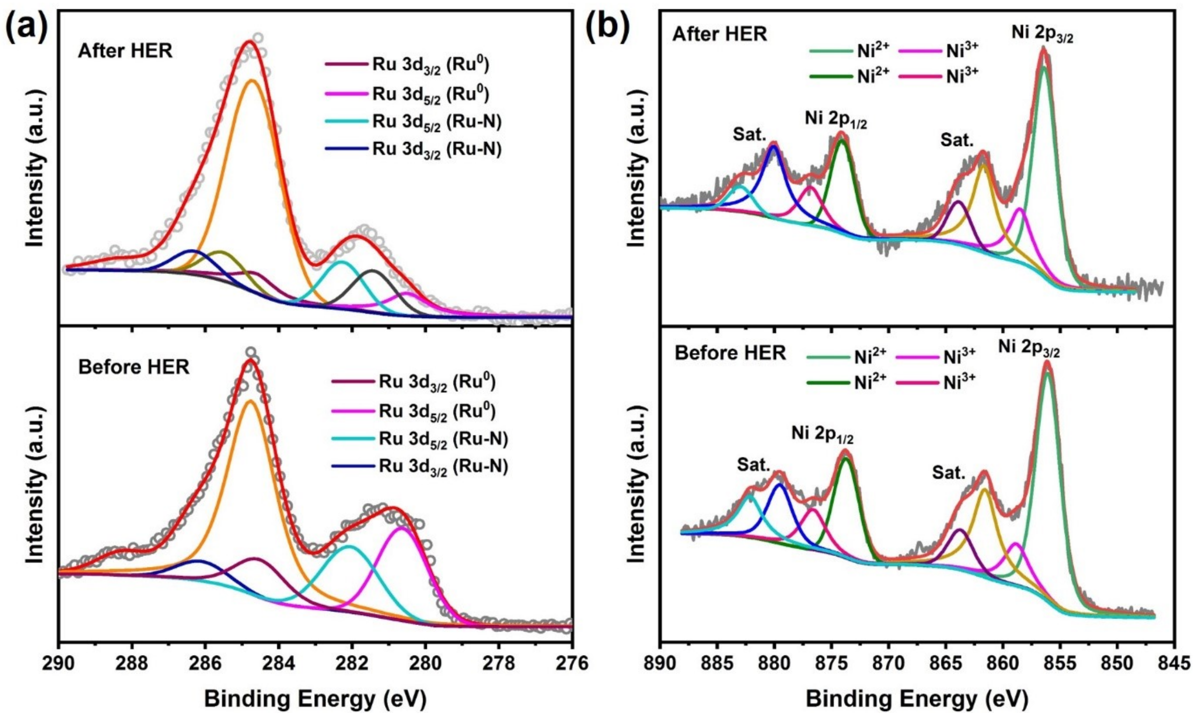

Figure S19 High resolution Ni 2p and Ru 3d of PANI-Ru@Ni_3S_2 (C 1s peaks omitted) before and after long-term stability test.

Table S1 Alkaline hydrogen evolution performance of Ni_3S_2-based hybrids formed on nickel foam

Catalysts	η@10 mA cm^{-2} (mV)	Tafel slope (mV dec^{-1})	Ref.
Ru@Ni_3S_2	19.8	33.2	This work
PANI-Ru@Ni_3S_2	24.5	36.5	
Pt nanoparticle-decorated Ni_3S_2 microrod Array	10	73	ACS Appl. Mater. Interfaces, 2020, 12:39163-39169.
N-doped Ni_3S_2	155	113	Adv. Energy Mater., 2018, 8: 1703538
Cu nanodots-decorated Ni_3S_2 nanotubes	128	76.2	J. Am. Chem. Soc., 2018, 140: 610-617
MoS_2/Ni_3S_2 Nanoarrays	76	56	ACS Appl. Mater. Interfaces, 2018, 10: 1752-1760
Ni_3S_2 films grown on nanoporous copper	60.8	67.5	Nano Energy, 2017, 36: 85-94.
N-anion decorated Ni_3S_2	110		Adv. Mater., 2017, 29: 1701584
Fe-doped Ni_3S_2 nanosheet array	47	95	ACS Catal. 2018, 8, 5431−5441
hollow MoOx/Ni_3S_2 composite microsphere	106	90	Adv. Funct. Mater., 2016, 26: 4839-4847
$Ni_xCo_{3-x}S_4$-decorated Ni_3S_2 nanosheet arrays	136	107	Nano Energy, 2017, 35: 161-170
CoSx/Ni_3S_2	204	133.32	ACS Appl. Mater. Interfaces, 2018, 10: 27712-27722
Nitrogen-doped carbon dots/ Ni_3S_2	160	127	Carbon, 2018, 129: 335-341
MoS_2−Ni_3S_2 Heteronanorods	98	61	ACS Catal., 2017, 7: 2357-2366
Cu-doped Ni_3S_2 nanoparticles	121	86.2	Nanoscale, 2021, 13, 2456–2464
$Ni_3Sn_2S_2$ dots-decorated thin Ni_3S_2 nanosheets	53.2	73.2	Appl. Catal., B, 2020, 267: 118675
amorphous $NiWO_4$ nanoparticles-decorated Ni_3S_2	136	112	Appl. Catal., B, 2020, 274: 119120
$CoMo_2S_4$/Ni_3S_2	51	69	Chem. Commun., 2021, 57, 785--788
Ni_3S_2 nanosheets edged with MoS_2	78	68	Appl. Catal., B, 2020, 268: 118435
CoS_x-Ni_3S_2	120	141	Appl. Catal., B, 2020, 269: 118780
Ni_3S_2–MoS_2 nanowire arrays	99	65	Chem. Commun., 2020, 56: 2471-2474
δ-FeOOH/Ni_3S_2	106	82.6	J. Mater. Chem. A, 2020, 8: 21199–21207
Co_9S_8/Ni_3S_2 heterostructure nanowire arrays	128	97.6	Appl. Catal., B, 2019, 253: 246-252

Ni_3S_2/MnS	116	41	Appl. Catal., B, 2019, 257: 117899
MoS_2/Co_9S_8/Ni_3S_2	113	85	J. Am. Chem. Soc., 2019, 141: 10417-10430
$Ni(OH)_2$/Ni_3S_2 nanoforests	50	49	Appl. Catal., B, 2019, 242: 60-66

Table S2 Alkaline hydrogen evolution performance of Ru-based hybrids

Catalysts	η@10 mA cm^{-2} (mV)	Tafel slope (mV dec^{-1})	Ref.
Ru@Ni_3S_2	19.8	33.2	This work
PANI-Ru@Ni_3S_2	24.5	36.5	
Ru SAs and NPs anchored on defective carbon	18.8	35.8	Adv. Sci., 2021, 2004516
carbon fiber cloth supported RuNi nanoclusters	43	30.4	Nanoscale, 2021, 13: 13042-13047
two-dimensional RuBe nanosheets	34.8	28.9	Chem. Eng. J., 2021, 421: 129741
Ru nanoclusters supported on N/S doped macroporous carbon spheres	32	24	Nanoscale Adv., 2021, 3: 5068-5074.
Ru decorated hollow N-doped carbon matrix	49	37	J. Mater. Chem. A, 2021, 9: 13958-13966
Ru nanoparticles-anchored sponge-like WNO embedded in N-doped carbon layers	24	39.7	Nano Energy, 2021, 80, 105531.
RuP clusters encapsulated in N, P-doped carbon	15.6	31	Nano Res., 2021, 14: 4321-4327.
Ru nanoclusters on Co_3O_4 porous nanowire	30.96	69.75	Nano Energy, 2021, 85: 105940.
Ru cluster catalysts supported on $Ti_3C_2T_x$ MXene	96	159	J. Phys. Chem. Lett., 2021, 12: 8016-8023.
Phosphorus-modified ruthenium–tellurium dendritic nanotubes	35	30.8	J. Mater. Chem. A 2021, 9: 5026-5032.
Ru nanoclusters/N-doped graphene	25.9	32.6	Carbon, 2021, 183: 362-367.
ruthenium decorated on S, N-codoped carbon	14	28	J. Mater. Chem. A, 2021, 9: 16967-16973
Air plasma treated Ru doped CoNi-LDH	29	69	Small 2021, 2104323
Ru nanoparticles confined in 3D nitrogen-doped porous carbon	17	42	Appl. Catal., B, 2021, 280: 119412
Ru/RuO_2 hybrid nanoparticles on MoO_2	18	50	J. Colloid Interface Sci., 2021, 604: 508-516
Partially reduced Ru/RuO_2 composites	17	35	Energy Environ. Sci., 2021, 14: 5433-5443
Ru nanoparticles supported on partially reduced TiO_2	15	49	Nano Energy, 2021, 106211.
Ru Nanoparticles on Boron-Doped $Ti_3C_2T_x$ (MXene) Nanosheets	62.9	100	Small, 2021, 2102218

Ru nanoclusters anchored on B/N–doped graphene	14	28.9	Nano Energy, 2020, 68: 104301
Ru on NiFe-P nanosheets	44	80	Appl. Catal., B, 2020, 263: 118324
Defect-rich copper-doped Ruthenium hollow nanoparticles	25	50	Chem Asian J, 2020, 15: 2868-2872
Ru nanoclusters/porous carbon	21	46.6	Green Chem., 2020, 22: 835-842.

Table S3 XPS peak parameters of Ru, Ni and S species in Ru@Ni_3S_2

Species		B.E. (eV)	FWHM	Relative peak area (%)
Ru	Ru^0	280.5	1.35	46.9
	Ru^{3+}	281.6	1.35	53.1
Ni	Ni^0	852.8	1.12	3.8
	Ni^{2+}	856.5	2.68	82.3
	Ni^{3+}	859.3	2.68	13.9
S	S-Ni	162.2	1.4	100

Table S4 XPS peak parameters of Ru and Ni species in PANI-Ru@Ni_3S_2

Species		B.E. (eV)	FWHM	Relative peak area (%)
Ru	Ru^0	280.5	1.62	55.9
	Ru-N	282.1	1.62	44.1
Ni	Ni^{2+}	856.5	2.60	81.5
	Ni^{3+}	859.3	2.60	18.5

Table S5 XPS peak parameters of Ru and Ni species in PANI-Ru@Ni_3S_2 after stability test

Species		B.E. (eV)	FWHM	Relative peak area (%)
Ru	Ru^0	280.5	1.35	27.1
	Ru^{x+}	281.4	1.35	34.4
	Ru-N	282.1	1.35	38.5
Ni	Ni^{2+}	856.5	2.40	74.6
	Ni^{3+}	859.3	2.40	25.4